ISPEC Fen Bilimleri Enstitüsü Dergisi, 4(2):83-92 2025
ISPEC Journal of Science Institute, 4(2):83-92, 2025
DOI: https://doi.org/10.5281/zenodo.17973311

Microstructural and Dielectric Characterization of MgO-added Al_2O_3-based Ceramics in the Terahertz Range

Kagan Murat PURLU [1], Elif ISIK [2], Betul KAFKASLIOGLU YILDIZ [2], Kholoud ELMABRUK [*1]

[1] Sivas University of Science and Technology, Faculty of Engineering and Natural Sciences, Electric-Electronic Engineering Department, Sivas
[2] Sivas University of Science and Technology, Faculty of Engineering and Natural Sciences, Metallurgical and Materials Engineering Department, Sivas
Sorumlu Yazar (Corresponding author): elmabruk@sivas.edu.tr

Abstract
This study investigates the effect of MgO addition on the microstructural and dielectric properties of Al2O3 ceramics. The dielectric properties of Al2O3-based ceramics with MgO addition were investigated in the terahertz (THz) range. The fabricated ceramic composites are characterized utilizing THz time-domain spectroscopy (THz-TDS). The relative density reached 99.5% with the addition of MgO, while the particle size decreased significantly. Although microstructural analysis indicated a more homogeneous distribution, complete effectiveness could not be achieved. THz-TDS measurements revealed that MgO-added samples exhibited a higher dielectric constant, lower absorption coefficient, and reduced loss tangent. These findings confirm that, although MgO cannot entirely suppress grain growth, it effectively reduces dielectric losses and enhances the suitability of Al2O3-based ceramics for terahertz applications.

Research Article

Article History
Received: 29.09.2025
Accepted: 30.11.2025

Keywords
Terahertz,
Terahertz Time-Domain Spectroscopy,
Aluminium Oxide,
Dielectric Properties

1. Introduction

Terahertz (THz) radiation, typically defined in the frequency range of 0.1–10 THz, has attracted increasing attention in recent years due to its unique ability to penetrate many non-conductive materials while being non-ionizing and safe for biological tissues (Tonouchi, 2007). Owing to these properties, THz technology has found promising applications in fields such as biomedical imaging, security screening, non-destructive testing, wireless communications, and materials characterization. However, despite these broad prospects, the practical implementation of THz systems is often limited by the availability of suitable materials and components that can operate efficiently in this spectral region. Ceramic materials stand out as strong candidates for THz applications because of their high thermal stability, mechanical properties, and tunable dielectric properties. In particular, alumina (Al_2O_3)-based ceramics have been extensively investigated as substrates, dielectric components, and protective coatings for THz devices (Naftaly et al., 2009). Their relatively low dielectric loss, chemical stability, and compatibility with various processing methods, including additive manufacturing, make them highly attractive for the development of advanced THz components. Moreover, by tailoring their microstructure, porosity, or by introducing specific additives, the dielectric response of ceramics in the THz band can be significantly modified, opening pathways for both low-loss transmission components and high-resolution imaging systems.

Hakobyan et al. (2022) investigated the dielectric properties of Al_2O_3 ceramics with different porosity ratios (0, 5, 10, 15, and 20 vol.%) in the THz frequency range (0.4–2 THz). The study revealed a linear relationship between the porosity ratio of the samples and both the dielectric constant and the dielectric loss tangent in the THz frequency range. (Hakobyan et al., 2022). In another study, the densification, microstructure, and dielectric properties in the 0.3–1.5 THz frequency range of Al_2O_3-based ceramics containing samarium oxide (Sm_2O_3) and ZrO_2 additives separately and together were investigated. It was found that the addition of ZrO_2 increased the refractive index, whereas the addition of Sm_2O_3 reduced the losses. Therefore, Al_2O_3-based ceramics with ZrO_2 additives were emphasized as suitable for applications requiring higher confinement and enhanced resolution, whereas Sm_2O_3-added Al_2O_3 ceramics were indicated for applications where low losses are essential (Purlu et al., 2025). Palka et al. utilized THz radiation for the non-destructive evaluation of assess damage in Al_2O_3 ceramic ballistic armor samples. The THz-TDS technique was employed to determine the refractive indices of the materials, which were then used in simulations based on the transfer matrix method. Using the transfer matrix method, the THz signals reflected from the sample were accurately simulated, the thicknesses of the sample layers were determined, and hidden defects were successfully identified. Additionally, the THz-TDS has been reported as an effective method for the non-destructive 3D imaging of Al_2O_3-based ballistic armor (Pałka et al., 2024). The dielectric behavior of Al_2O_3 ceramics produced through a stereolithography-based additive manufacturing method was investigated by Ornik et al. The study determined the refractive index and absorption coefficient of Al_2O_3 ceramics in a wide frequency range (0.3–2.5 THz). It was reported that samples produced via additive manufacturing exhibit a high refractive index ($n>3$) and a low absorption coefficient (<2 cm^{-1} at 1 THz), highlighting the broad opportunities offered by additive manufacturing for implementing complex structures and compact devices in the THz frequency range (Ornik et al., 2021).

In this study, the dielectric properties of MgO-added Al_2O_3-based ceramics prepared by dry pressing were systematically investigated in the THz frequency range. This work uniquely focuses on the THz dielectric loss behavior of MgO-modified Al_2O_3, a topic that has not been systematically examined in the existing literature. In addition, the densification

and microstructural characteristics of the samples were analyzed to explore the correlation between their microstructure and dielectric response. The results are presented in a comparative manner between pure Al_2O_3 and MgO-added compositions.

2. Material and Method

2.1. Sample preparation and microstructural characterization

In this study, the raw materials were α-Al_2O_3 powder (purity 99.95%, 0.25-0.45 average grain size, Alfa Aesar), magnesium nitrate ($Mg(NO_3)_2.6H_2O$, Sigma Aldrich) as the MgO source, polyacrylic acid (Darvan 821A, MSE Tech Co. Ltd., Turkey) as the dispersant, polyvinyl alcohol as the binder (PVA, binder, Sigma Aldrich), and glycerol as the plasticizer (Sigma Aldrich). For the fabrication of pure Al_2O_3 samples, α-Al_2O_3 powder and 0.5 wt% dispersant were ball-milled in distilled water for 24 hours. A binder solution containing 2 wt% polymer was added to the ball-milled powder. Subsequently, the prepared powder mixture was dried, ground in an agate mortar, and granulated by sieving through a 90 μm mesh. For the samples containing MgO, the ball-milled and dried powder mixture with magnesium nitrate was calcined at 800 °C for 2 h before the binder solution was added. Through this calcination process, MgO was obtained from the $Mg(NO_3)_2.6H_2O$ source. To provide a homogeneous distribution of MgO in the microstructure, MgO was obtained through calcination from the $Mg(NO_3)_2.6H_2O$ source instead of using MgO powder directly. After the calcination process, the binder solution was added to the powder mixture, followed by drying, grinding, and sieving. The granulated powders were initially shaped using a uniaxial press at 40 MPa and subsequently subjected to cold isostatic pressing at 200 MPa. The production parameters were determined based on the results of previous studies (Taşdemir et al., 2023; Kafkaslıoğlu Yıldız et al., 2024; Usta et al., 2024).

The pressed samples were exposed to a binder burn-out process at 600°C for 2 hours, then pressureless sintered at 1600°C for 2 hours in air atmosphere. A lapping process was applied to grind and parallelize the surfaces of the sintered samples. The density of the fabricated samples was determined via Archimedes' method. The relative density is calculated as the ratio of the experimental density to the theoretical density of the ceramic sample. The theoretical densities of the MgO-added samples were calculated according to the mixing rule. For microstructural analysis, the samples were thermally etched for 90 min at 1500°C. The microstructural analysis of the thermally etched samples was carried out using scanning electron microscopy (SEM). The grain size measurements were also performed on SEM images using the linear intercept method (Usta et al., 2024).

2.2. Dielectric properties characterization

The dielectric properties of the ceramic samples were investigated using a terahertz time-domain spectroscopy (THz-TDS) system operating in transmission mode. In this technique, ultrafast femtosecond laser pulses generate broadband THz radiation, which is transmitted through the sample, and the transmitted electric field is directly recorded in the time domain. This allows simultaneous access to both amplitude and phase information of the THz wave, enabling the extraction of complex dielectric parameters without relying on Kramers–Kronig relations. In the present study, measurements were performed using a Toptica Photonics TeraFlash Pro system, which provides a dynamic range of approximately 95 dB and a spectral bandwidth extending up to 6 THz. The setup includes a high-precision mechanical delay stage capable of scanning a 50 ps time window, recording up to 60 temporal waveforms per second. Prior to each measurement, a reference spectrum was recorded. The collected time-domain signals were converted into frequency-domain spectra via fast Fourier transform (FFT). From these spectra, the complex refractive index $\tilde{n}$

$(\omega)=n(\omega)+i\kappa(\omega)$ was determined, where $n(\omega)$ is the real refractive index and $\kappa(\omega)$ is the extinction coefficient. The absorption coefficient was calculated from (Purlu et al., 2025):

$$\alpha(\omega)=2\omega\kappa(\omega)/c \quad \textbf{1)}$$

where c is the speed of light. The real part of permittivity was obtained from $\varepsilon'(\omega)\approx n2(\omega)$, while the imaginary part $\varepsilon''(\omega)$ was derived from the extinction coefficient. The dielectric loss tangent was then calculated as (Purlu et al., 2025):

$$\tan\delta=\varepsilon''/\varepsilon' \quad \textbf{2)}$$

Sample thicknesses were precisely measured with a micrometer (accuracy ±5 μm) and incorporated into the calculations. Data analysis was carried out using a custom MATLAB routine to extract frequency-dependent refractive index, permittivity, absorption coefficient, and loss tangent in the 0.3–1 THz range.

3. Results and Discussion

3.1. Density measurement and microstructural analysis

Table 1 presents the relative density and grain size values of the pure Al_2O_3 and Al_2O_3-MgO samples (abbreviated as AlMgO). Based on the results, the relative density increased from 98.9% to 99.5% after the addition of MgO. This indicates that the MgO additive acts as a sintering aid and enhances densification. A similar effect was observed in the grain size, which was found to decrease with the addition of MgO. The high sintering temperature (1600°C) resulted in grain growth in the pure Al_2O_3 sample. It can be seen in the SEM images in Fig. 1 that the grain size distributions of the pure Al_2O_3 samples are not homogeneous, with large grains forming alongside very fine grains. It was observed that, with the addition of MgO, the grain size decreased to 4.1 μm and the grain size distribution became more uniform compared to that of pure Al_2O_3. However, despite the decrease in grain size in AlMgO samples, the presence of large grains in the microstructure indicates that MgO was not entirely effective with the possibility of not being sufficiently homogeneously distributed. The literature reports that the addition of MgO inhibits grain growth, resulting in a finer, more homogeneous, and denser microstructure. Consistent with these literature findings, the present study observed a reduction in grain size and an increase in densification with the addition of MgO (Rittidech et al., 2006; Yang et al., 2024).

Table 1. Relative density and grain size values of the samples

Composition	Relative Density (%)	Grain size (μm)
Pure Al_2O_3	98.9	8.0
AlMgO	99.5	4.1

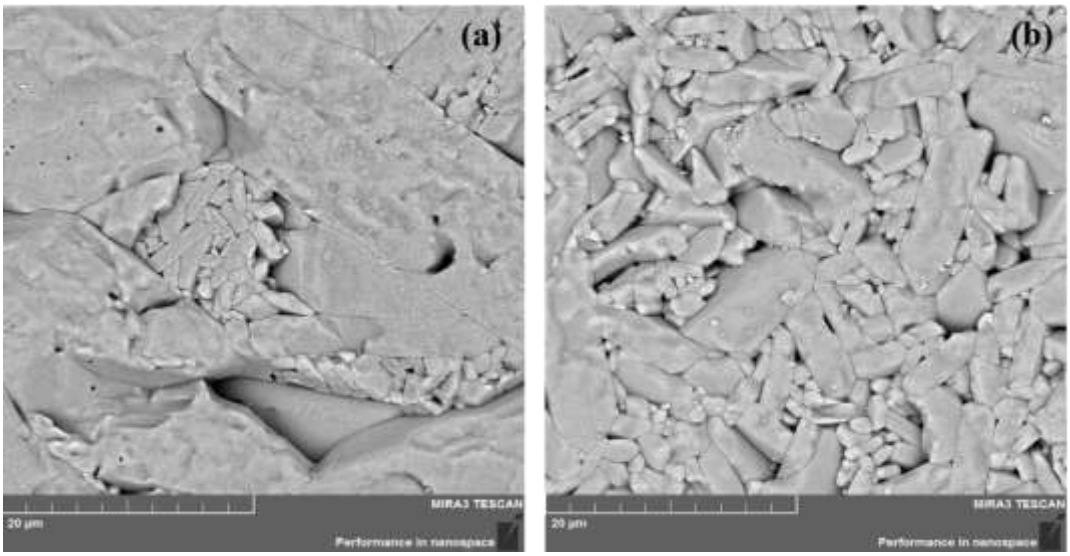

Figure 1. SEM images of the pure a) Al_2O_3 and b) AlMgO samples sintered at 1600°C for 2 h

3.2. Dielectric properties characterization

The THz-TDS measurements provided a comprehensive dataset on the dielectric response of the prepared ceramic samples, allowing the frequency-dependent refractive index, absorption coefficient, and dielectric function to be extracted. By comparing the spectral features of Al_2O_3 and AlMgO ceramics, clear trends associated with compositional modifications and microstructural effects could be observed (Gao et al., 2025). These results form the basis for the following discussion, where the impact of additive, porosity, and additive engineering on the THz optical properties of ceramics is analyzed in detail, with particular attention to their potential role in practical THz device applications.

The refractive index spectra of Al_2O_3 and AlMgO ceramics in the 0.3–1.0 THz frequency range are shown in Fig. 2. Both materials exhibited relatively stable refractive indices with only a slight frequency dispersion. Pure Al_2O_3 maintained values around $n \approx 3.05$, which is consistent with previously reported values for dense alumina ceramics (Ma et al., 2019). In contrast, the AlMgO ceramic displayed slightly higher refractive index values across the entire frequency range, starting from ~3.3 at 0.3 THz and gradually decreasing toward ~3.1 at 1.0 THz. This enhancement suggests that Mg incorporation into the alumina lattice modifies the polarization response of the material, possibly by influencing grain boundary phases and improving densification. The weak downward trend with frequency, observed in both samples, reflects normal dielectric dispersion, where the refractive index approaches a constant value at higher THz frequencies. The higher refractive index of AlMgO compared to pure Al_2O_3 indicates an increase in effective permittivity (since $\varepsilon' \approx n^2$), suggesting that Mg substitution enhances the polarizability of the ceramic matrix. This behavior highlights AlMgO as a promising candidate for THz applications requiring materials with slightly higher dielectric constants and stable refractive index behavior.

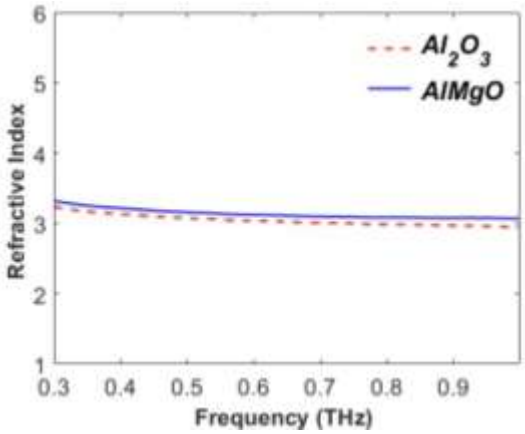

Figure 2. Refractive index of the ceramic samples in the THz range.

The absorption coefficient spectra of Al_2O_3 and AlMgO ceramics in the 0.3–1.0 THz range are presented in Fig. 3. Both materials showed an increasing absorption with frequency, consistent with typical phonon-related loss mechanisms in the THz region. Pure Al_2O_3 exhibited significantly higher absorption values compared to AlMgO, exceeding 20 cm^{-1} at 1.0 THz. In contrast, AlMgO ceramics displayed lower absorption coefficients across the entire spectrum, remaining below 15 cm^{-1} at the upper frequency limit. At low frequencies (<0.5 THz), the difference between the two materials was minimal; however, as the frequency increased, the separation became more pronounced. This indicates that Mg incorporation into the alumina lattice effectively suppresses high-frequency scattering and reduces vibrational losses (Gao et al., 2025). This reduction in absorption in AlMgO can be directly linked to the microstructural modifications induced by MgO. As reported in previous studies, Mg addition inhibits abnormal grain growth and promotes a finer and more densely packed microstructure. (Rittidech et al., 2006; Yang et al., 2024). In our samples as well, grain refinement and improved densification were observed. Such microstructural refinement reduces phonon–boundary scattering and suppresses defect-mediated vibrational damping, both of which contribute to THz absorption. Consequently, fewer high-frequency scattering pathways are available in AlMgO, leading to a lower overall absorption coefficient. Therefore, the observed trends confirm that Mg incorporation effectively mitigates phonon-related loss processes, making AlMgO a lower-loss dielectric material than pure Al_2O_3, particularly for applications operating above 0.7 THz.

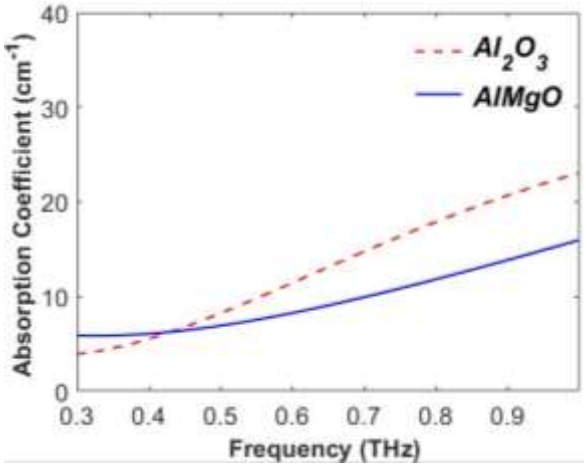

Figure 3. Absorption coefficient of the ceramic samples in the THz range.

The dielectric loss tangent spectra of Al_2O_3 and AlMgO ceramics are shown in Fig. 4. Pure Al_2O_3 exhibited tan δ values in the range of 0.05–0.1, with a gradual increase as the frequency approached 1.0 THz. This frequency-dependent rise in dielectric losses can be attributed to enhanced phonon–polariton interactions and extrinsic scattering from grain boundaries and residual porosity. By contrast, the AlMgO ceramic consistently demonstrated lower loss tangent values across the entire frequency range, remaining below 0.05 even at 1.0 THz. At low frequencies (<0.5 THz), AlMgO maintained tan δ values around 0.02–0.03, almost half of that measured for pure Al_2O_3. This reduction indicates that Mg incorporation effectively suppresses dielectric dissipation mechanisms (Wang et al., 2013). The reduction in dielectric loss observed in AlMgO can be directly linked to the microstructural improvements induced by MgO addition. As shown in previous studies, Mg suppresses abnormal grain growth and promotes a finer, more homogeneous, and denser microstructure. In our samples as well, a noticeable decrease in grain size and an increase in densification were observed. Such microstructural refinement reduces the density of scattering centers, enhances grain-boundary continuity, and limits defect-mediated polarization processes. These improvements effectively suppress phonon–boundary scattering and defect-related relaxation mechanisms both of which play major roles in dielectric dissipation in the THz regime. Therefore, the lower tan δ values in AlMgO confirm that Mg incorporation mitigates phonon–polariton damping and diminishes defect-assisted energy loss pathways. Overall, these results demonstrate that Mg-modified alumina ceramics provide a more favorable low-loss dielectric response in the THz region, making them better suited for THz applications where dielectric transparency and minimal energy dissipation are critical.

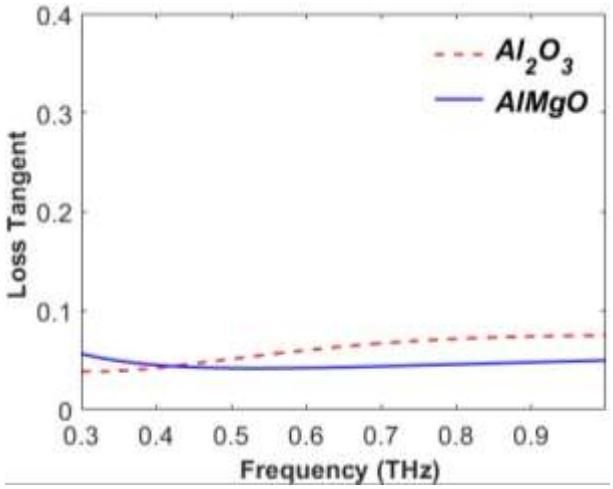

Figure 4. Loss tangent (tan δ) of the ceramic samples in the THz range.

The real part of the dielectric permittivity (ε′) of Al_2O_3 and AlMgO ceramics is illustrated in Fig. 5. Pure Al_2O_3 exhibited permittivity values around 9–9.5 in the measured range, which aligns with previously reported values for dense alumina ceramics in the THz regime (Ma et al., 2019). A mild frequency-dependent decrease was observed, with ε′ gradually decreasing from ~9.5 at 0.3 THz to ~8.7 at 1.0 THz. In contrast, AlMgO ceramics consistently displayed higher permittivity values, starting from ~11 at 0.3 THz and converging to ~9.8 at 1.0 THz. This enhancement in permittivity directly correlates with the observed increase in refractive index, as $\varepsilon' \approx n^2$, and suggests that Mg incorporation improves the polarization capacity of the ceramic. The elevated ε′ values may be attributed to enhanced densification and reduced porosity in the AlMgO structure, as well as the

possible contribution of Mg–O bonds to lattice polarizability. The frequency dispersion in both samples reflects typical dielectric behavior, where permittivity decreases with frequency due to the reduced contribution of dipolar polarization at higher THz frequencies. Nevertheless, the higher ε′ values of AlMgO across the entire spectrum indicate that Mg modification of alumina enables tuning of the dielectric constant while maintaining relatively low losses, as confirmed by the corresponding loss tangent spectra.

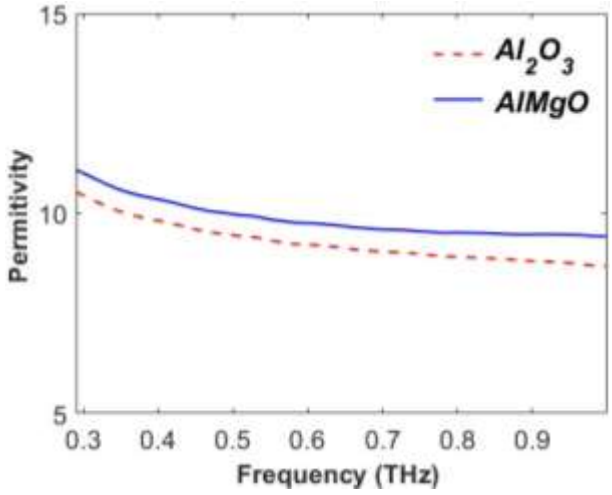

Figure 5. Dielectric permittivity (ε′) of the ceramic samples in the THz range.

Overall, the comparative THz characterization of Al_2O_3 and AlMgO ceramics demonstrates that Mg incorporation substantially modifies the dielectric response of alumina in the 0.3–1.0 THz range. AlMgO exhibited slightly higher refractive index and permittivity values compared to pure alumina, indicating enhanced polarization capability. More importantly, the absorption coefficient and dielectric loss tangent of AlMgO were consistently lower, particularly at higher frequencies, suggesting reduced phonon-related dissipation and minimized scattering from microstructural defects. These improvements are attributed to the stabilizing role of Mg in the alumina lattice, which enhances densification and suppresses extrinsic loss pathways. Consequently, AlMgO ceramics combine moderately higher permittivity with significantly reduced absorption and loss, making them promising candidates for terahertz components such as substrates, lenses, and waveguides where low-loss and stable dielectric performance are essential (Meeporn et al., 2023).

4. Conclusion

In the presented work, the densification, microstructural characteristics, and dielectric properties in the THz band of the pure Al_2O_3 and MgO-added Al_2O_3 ceramics were investigated. The relative density of samples prepared by dry pressing increased to 99.5% and the particle size decreased to 4.1 μm after the addition of MgO. Compared to the pure Al_2O_3, the grain size was found to be reduced by 48.7%. Microstructural images revealed that the addition of MgO resulted more homogeneous grain size and morphology compared to the pure Al_2O_3. However, due to the possibility of insufficiently homogeneous distribution, large grains were still present in the microstructure, and therefore MgO could not be entirely effective. The THz-TDS results further demonstrated the influence of MgO addition on the dielectric response. The refractive index of AlMgO ceramics remained slightly higher than that of pure Al_2O_3 across the measured frequency range, indicating enhanced permittivity values. More importantly, the absorption coefficient of the MgO-added samples was significantly lower, particularly at higher frequencies, leading to a

substantial reduction in dielectric losses. This trend was also confirmed by the dielectric loss tangent, which showed consistently lower values for AlMgO ceramics compared to pure Al_2O_3, highlighting their superior low-loss performance. Furthermore, the real part of the permittivity was found to be higher and more stable in the MgO-added samples, suggesting improved dielectric uniformity. These results confirm that while MgO addition alone cannot completely suppress grain coarsening, it effectively tailors the dielectric properties, reducing losses and enhancing the suitability of Al_2O_3-based ceramics for terahertz applications.

References

Gao, C., Zheng, Z., Ke, S., Guan, B., He, Q., 2025. Optical–dielectric characterization and contactless thickness measurement of ceramics based on terahertz spectroscopy. *Applied Optics*, 64(19): 5302–5310.

Hakobyan, D., Hamdi, M., Redon, O., Ballestero, A., Mayaudon, A., Boyer, L., Durand, O., & Abraham, E., 2022. Non-destructive evaluation of ceramic porosity using terahertz time-domain spectroscopy. *Journal of the European Ceramic Society*, 42(2): 525–533.

Kafkaslıoğlu Yıldız, B., Taşdemir, S., Işık, E., Tür, Y.K., 2024. Assessing the fracture toughness of Al2O3-Sm2O3 ceramics for different Sm2O3 contents using a reliable toughness measurement method: single-edge precracked beam. *Journal of Materials Engineering and Performance*, 34(11): 9618-9626.

Ma, M., Wang, Y., Navarro-Cía, M., Liu, F., Zhang, F., Liu, Z., Li, Y., Hanham, S.M., Hao, Z., 2019. The dielectric properties of some ceramic substrate materials at terahertz frequencies. *Journal of the European Ceramic Society*, 39(14): 4424–4428.

Naftaly, M., Greenslade, P.J., Miles, R.E., Evans, D., 2009. Low-loss nitride ceramics for terahertz windows. *Optical Materials*, 31(11): 1575–1577.

Ornik, J., Sakaki, M., Koch, M., Balzer, J.C., Benson, N., 2021. 3D Printed Al2O3 for Terahertz Technology. *IEEE Access*, 9: 5986–5993.

Pałka, N., Kamiński, K., Maciejewski, M., Pacek, D., Świderski, W., 2024. Terahertz nondestructive testing of alumina-based ceramic ballistic protection armor. *Infrared Physics and Technology*, 137.

Purlu, K.M., Dalgac, S., Isik, E., Yildiz, B.K., Elmabruk, K., 2025. Preparation and dielectric properties of Al2O3-based ceramic composites with Sm2O3 and ZrO2 additives for terahertz applications. *Ceramics International*.

Rittidech, A., Portia, L., Bongkarn, T., 2006. The relationship between microstructure and mechanical properties of Al_2O_3–MgO ceramics. *Materials Science and Engineering A*, 438: 395–398.

Purlu, K.M., Dalgac, S., Korkut, I., Elmabruk, K., 2025. Synthesis, fabrication and characterization of 3D printable photopolymer resins for terahertz applications. *Journal of Materials Science: Materials in Electronics*, 36(22): 1395.

Taşdemir, S., Kafkaslıoğlu Yıldız, B., Işık, E., Tür, Y., 2023. Exploring microstructure and bending strength of Al2O3 ceramics doped with Sm2O3 rare-earth oxide: impact of volume ratios and sintering temperatures. *Karadeniz Fen Bilimleri Dergisi*, 13(4): 1581–1594.

Tonouchi, M., 2007. Cutting-edge terahertz technology. *Nature Photonics*, 1(2): 97–105.

Usta, U., Kafkaslıoğlu Yıldız, B., Dara, B.G., 2024. The effect of sintering temperature and low content of TiO2 on the microstructure and mechanical properties of ZTA-TiO2 composites. *Journal of the Australian Ceramic Society*, 60(1): 35–45.

Purlu, K.M., Dalgac, S., Isik, E., Yildiz, B.K., Elmabruk, K., 2025. Impact of pure α-Al2O3 powder sources and sintering temperature on the behaviour of Al2O3 ceramics in Terahertz band. *Journal of the Australian Ceramic Society*, 1-9.

Wang, H., Li, W., Ternström, C., Lin, H., Shi, J., 2013. Effect of Mg doping on microwave dielectric properties of translucent polycrystalline alumina ceramic. *Ceramics International*, 39(2): 1583–1586.

Yang, S., Wei, P., Dai, Y., Liu, S., Han, N., Fu, X., Fan, L., Zhang, M., An, L., 2024. Effects of MgO doping concentration on densification and microstructure of flash sintered alpha-Al_2O_3 ceramics. *Journal of the European Ceramic Society*, 44: 4210–4215.